Experimental and Kinetic Modeling Study of the Effect of NO and SO_2 on the Oxidation of CO–H_2 Mixtures

PHILIPPE DAGAUT,[1] FRANCK LECOMTE,[1] JACOB MIERITZ,[2] PETER GLARBORG[2]

[1]CNRS, *Laboratoire de Combustion et Systèmes Réactifs*, 1C, *Avenue de la Recherche Scientifique*, F-45071 *Orléans Cedex* 2, *France*
[2]*Department of Chemical Engineering*, *Technical University of Denmark*, DK-2800, *Lyngby*, *Denmark*

Received 10 February 2003; accepted 23 June 2003

DOI 10.1002/kin.10154

ABSTRACT: The effect of NO and SO_2 on the oxidation of a CO–H_2 mixture was studied in a jet-stirred reactor at atmospheric pressure and for various equivalence ratios (0.1, 1, and 2) and initial concentrations of NO and SO_2 (0–5000 ppm). The experiments were performed at fixed residence time and variable temperature ranging from 800 to 1400 K. Additional experiments were conducted in a laminar flow reactor on the effect of SO_2 on CO–H_2 oxidation in the same temperature range for stoichiometric and reducing conditions. It was demonstrated that in fuel-lean conditions, the addition of NO increases the oxidation of the CO–H_2 mixture below 1000 K and has no significant effect at higher temperatures, whereas the addition of SO_2 has a small inhibiting effect. Under stoichiometric and fuel-rich conditions, both NO and SO_2 inhibit the oxidation of the CO–H_2 mixture. The results show that a CO–H_2 mixture has a limited NO reduction potential in the investigated temperature range and rule out a significant conversion of HNO to NH through reactions like HNO + CO ⇔ NH + CO_2 or HNO + H_2 ⇔ NH + H_2O. The chain terminating effect of SO_2 under stoichiometric and reducing conditions was found to be much more pronounced than previously reported under flow reactor conditions and the present results support a high rate constant for the H + SO_2 + M ⇔ HOSO + M reaction. The reactor experiments were used to validate a comprehensive kinetic reaction mechanism also used to simulate the reduction of NO by natural gas blends and pure C_1 to C_4 hydrocarbons.
 Int J Chem Kinet 35: 564–575, 2003

INTRODUCTION

Nitrogen oxides (NO_x), responsible for acid rain, are emitted from both stationary and mobile combustion systems. Among technologies used to control emissions of NO_x from stationary combustion devices, one finds reburning, a low-cost and effective technique,

Correspondence to: Philippe Dagaut; e-mail: dagaut@cnrs-orleans.fr.
Contract grant sponsor: Joule Project ABRICOS.
Contract grant number: ENK6-CT2000-00324.

already in use [1,2]. It is basically a staged combustion: in the primary stage, the fuel is burned in fuel-lean to stoichiometric conditions producing NO_x; in the secondary stage, the reburning zone, a secondary fuel is added to turn the mixture fuel-rich and facilitate NO_x reduction; and in the third stage, the burnout zone, additional air is injected to complete the combustion. Nitrogen-containing intermediates are formed in the reburning zone, particularly cyanides and amines. These species are oxidized in the burnout zone, forming N_2 or regenerating NO.

Several recent studies were devoted to the establishment of a kinetic scheme for reburning using various fuels [3–6]. However, the chemistry involved in reburning is very complex and to develop a reliable mechanism further experimental and computational studies are required, particularly at moderate temperatures (<1800 K). Recent interest in reburning has focused on the use of solid fuels, from coal to biomass, as reburn fuels. In particular, reburning with biomass has received attention, since biomass is considered to be CO_2 neutral. The use of solid reburn fuels introduces another complexity, since they contain chemically bound sulfur. Biomass such as wood or straw contains generally less sulfur than coal, although high concentrations were reported in the literature [7–10]. It has been shown that SO_2 may have a significant effect on the chemistry involved in reburning [11–13], but this interaction is not fully understood.

The pyrolysis of biomass yields mostly CO and H_2 at high temperatures [9,10,14–16]. Although these reactants were previously shown to have a limited reduction potential toward NO under flow reactor conditions at moderate temperatures [12], confirmation of these results under a broader range of conditions is desirable. Thus, as part of a continuing effort in these laboratories to obtain a better understanding of the chemical kinetics of fuel oxidation and interaction with NO_x and SO_x, a series of experiments was performed using several simple reburn fuels. The results obtained for the reaction of NO and SO_2 with a CO–H_2 mixture are presented here together with detailed chemical kinetic modeling. Avoiding the complications of the presence of hydrocarbons, these results also serve to increase our knowledge of nitrogen and sulfur chemistry in combustion. Both a jet-stirred reactor and a flow reactor were used in the investigation. Of particular interest was the potential reduction of NO at moderate temperatures through a pathway involving conversion of HNO to NH by reaction with H_2 and CO. Such a reaction pathway is supported by direct measurements of NH + CO_2 and NH + H_2O [17], but appears to be inconsistent with results from flow reactors [18] and laminar diffusion flames [19]. A second issue is the effect of SO_2 on the radical pool. Under reducing conditions, presence of SO_2 is believed to catalyze H atom recombination by the reaction sequence H + SO_2 + M $\Leftrightarrow$ HOSO + M, HOSO + H $\Leftrightarrow$ SO_2 + H_2. The importance of this mechanism is presently controversial, because proposed rate constants for the H + SO_2 recombination reaction derived from theory [20], from low-pressure premixed flames [21], and from flow reactor experiments [22] vary by more than an order of magnitude.

EXPERIMENTAL

Most of the experiments performed in this study were conducted in a fused-silica jet-stirred reactor (JSR). It has been presented in detail elsewhere [4,23] and will only be reviewed briefly here. A 40-mm o.d. spherical sphere equipped with four injectors having nozzles of 1 mm i.d., for the admission of the gases achieving the stirring, constitutes the JSR. The JSR is located inside a regulated electrical resistance system of $\simeq$1.5 kW, surrounded by insulating material; it operates at atmospheric pressure. The reburn fuel, NO, SO_2, and oxygen flow rates are measured and regulated by thermal mass-flow controllers. These high-purity gases (>99.9%) are diluted by a flow of nitrogen (<50 ppm of O_2 and H_2O; <1000 ppm of Ar; <5 ppm of H_2) and mixed at the entrance of the injectors after preheating. A molecular sieve 5 Å and a cooled trap were used on the fuel line to avoid sending eventual traces of $Fe(CO)_5$, a well-known contaminant of CO cylinders.

According to previous residence time distribution studies, the reactor used in this work is operating under macro-mixing conditions such that a perfectly stirred reactor model can be used for the modeling of these experiments. The mixing time, a crucial parameter for NO reburning, was much shorter than the residence time in the reactor (by about a factor of 70 at least). Furthermore, great care was taken in this series of experiments to minimize the reactions in the mixing zone: the contact time in the mixing zone was kept minimal compared to the residence time in the reactor. Consequently, even at the highest temperatures of this study no evidence for reactions of NO occurring in the mixing zone could be found. As observed in previous studies [4,23], a good thermal homogeneity was obtained for each experiment along the whole vertical axis of the reactor. That was measured using a Pt/Pt–Rh10% thermocouple of 0.1 mm diameter located inside a thin-wall fused-silica tube (<0.5 mm), in order to prevent catalytic reactions on the wires. Because of the high degree of dilution used in these experiments, the temperature rise due to the reaction was $\leq$20 K and no flame

occurred in the JSR. Typical temperature variations of $\leq$8 K along the vertical axis of the JSR have been measured in the present work. Low pressure samples of the reacting mixture ($\approx$30 Torr) were taken using a sonic quartz probe, for immediate gas chromatography (GC) analyses. In order to improve the GC detection, these samples were pressurized at 1 bar, before injection into the GC column, using an homemade piston. Capillary columns of 0.53 mm i.d. (Poraplot U and molecular sieve 5 Å) were used with a thermal conductivity detector (TCD) for measurements of permanent gases (hydrogen, oxygen, carbon monoxide, and carbon dioxide). On-line Fourier transform infrared (FTIR) analyses of the reacting gases were also performed by connecting the exit of the sampling probe to a thermally regulated Teflon line (140°C) fitted to a thermally regulated (120°C) FTIR cell. H_2O, NO, NO_2, N_2O, NH_3, HCN, CO, CO_2, and SO_2 could be measured by FTIR. Beside NO, no N-species could be measured since they were below the detection limit (around 1 ppm). These low concentrations were confirmed by the kinetic modeling. Very good agreement between the GC and FTIR analyses was found for the compounds measured by both techniques (CO, CO_2). Carbon balance checked for every sample was found good within $\leq$5%.

In addition to the JSR experiments, data were obtained from experiments in a laminar flow reactor (LFR). This reactor has been designed to approximate plug flow in the laminar flow regime. The flow reactor setup and the experimental procedure are described in detail elsewhere [24] and only a brief description is given here. The gaseous components were fed to the reactor in four streams, which were preheated separately. The main flow contained nitrogen, oxygen, and water, while other reactants were fed through smaller injector tubes. All reactants were mixed within 5 ms at the entrance to the reaction zone. The reactor tube had a radius of 0.45 cm and a length of 19 cm. The temperature was measured by a thermocouple placed in a quartz tube with no access for the reactant gases. The gas flow was kept constant during an experiment, with the residence time (approximately 200 ms) depending on the temperature in the reaction zone. The product gas was quenched at the outlet of the reactor by heat exchange with cooling air. The concentrations of CO, CO_2, and O_2 were measured continuously by infrared and paramagnetic analyzers with an accuracy of 3% but no less than 5 ppmv.

KINETIC MODELING

The stirred reactor computations were carried out using the PSR computer code [25], which computes species concentrations from the balance between the net rate of production of each species by chemical reaction, and the difference between the input and output flow rates of species. The flow reactor results were modeled with SENKIN [26], which performs an integration in time, and with CRESLAF [27], which allows for two-dimensional boundary-layer calculations with surface chemistry. The results of the SENKIN calculations were compared to experimental data using the nominal residence time in the reactor. CRESLAF solves the mass conservation and boundary-layer equations that describe the fluid flow coupled with species equations describing chemical reaction and both convective and diffusive transport of species. PSR, SENKIN, and CRESLAF run in conjunction with the CHEMKIN subroutine library [28]; CRESLAF further draws on the SURFACE CHEMKIN package [29].

The reaction mechanism used in this study is mainly drawn from a comprehensive chemical kinetic model for the reduction of NO by natural gas blends in simulated reburning conditions [4]. This scheme represents an updated version of a kinetic mechanism used previously to describe oxidation of methane, ethane, ethylene, propane, propene, acetylene, and natural gas [30,31]. Recently, the NO_x submechanism has been updated by including the low-temperature chemistry involved in hydrocarbon–NO mutual sensitization [4]. In the present work, rate constants for a few reactions in this subset were updated, including NO + OH + M = HONO + M [5], $H_2NO + M = HNO + H + M$ [9], and $NO_2 + HO_2 = HONO + O_2$ [32]. In addition to the present data, this part of the mechanism was tested with good results against experimental data for the reduction of NO by C_1 to C_4 hydrocarbons, including a natural gas blend (methane–ethane 10:1), and for the low-temperature interactions between NO and simple alkanes.

The SO_x submechanism and the corresponding thermochemistry were largely taken from Glarborg and coworkers [22,33]. The only exception concerns the reaction $H + SO_2 + M \Leftrightarrow HOSO + M$, and the thermochemistry of HOSO. In the present work, we found that a fast rate for the $H + SO_2$ recombination reaction was required to explain the experimental results. The low rate constant derived by Alzueta et al. [22] appears to be inconsistent with the present results, and we have adopted the value derived theoretically by Goumri et al. [20] together with their thermochemistry for HOSO, assuming the reaction proceeds at its low pressure limit. This issue is discussed further below.

Rate coefficients for key reactions in the nitrogen and sulfur subset are listed in Table I, while Table II contains thermodynamic data for key species. The

Table I Rate Coefficients for Key Reactions in the Reaction Mechanism

Reaction	A	β	E	Reference
(7) $SO_2 + O\,(+M) = SO_3\,(+M)$	9.2×10^{10}	0.0	2,384	[22]
Low pressure limit:	4.0×10^{28}	−4.0	5,250	
(8) $SO_2 + OH\,(+M) = HOSO_2\,(+M)$	7.2×10^{12}	0.0	715	[22]
Low pressure limit:	4.5×10^{26}	−3.3	715	
Troe centering:	0.70	1×10^{-30}	1×10^{30}	
(14) $HOSO + H = SO_2 + H_2$	3.0×10^{13}	0.0	0	[22]
(57) $HOSO + O_2 = HO_2 + SO_2$	1.0×10^{12}	0.0	1,000	[22]
(58) $H + SO_2 + M = HOSO + M$	2.1×10^{31}	−4.4	10,810	[20], This work
(64) $HOSO_2 + O_2 = HO_2 + SO_3$	7.8×10^{11}	0.0	656	[22]
(85) $NH + OH = HNO + H$	2.0×10^{13}	0.0	0	[4]
(126) $HNO + H = NO + H_2$	4.4×10^{11}	0.72	650	[4]
(141) $NO + HO_2 = NO_2 + OH$	2.1×10^{12}	0.0	−480	[4]
(142) $NO + OH + M = HONO + M$	2.0×10^{12}	−0.05	−721	[5]
(143) $NO + H + M = HNO + M$	2.3×10^{18}	−0.9	0	[4]
(146) $NO_2 + H = NO + OH$	1.0×10^{14}	0.0	362	[4]
(150) $NO_2 + HO_2 = HONO + O_2$	6.3×10^{8}	1.25	5,000	[32]
(a) $HNO + CO = NH + CO_2$		Slow		This work
(b) $HNO + H_2 = NH + H_2O$		Slow		This work

The Arrhenius parameters are given in cm, mol, s, cal/mol for $k = AT^{\beta} \exp(-E/RT)$. Third body efficiencies: N_2: 1.0; SO_2: 10; H_2O: 10.

full reaction mechanism used here, including references and thermochemical data, is available from the authors (dagaut@cnrs-orleans.fr). The rate constants for reverse reactions were computed from the forward rate constants and the equilibrium constants, using appropriate thermochemical data [34–36].

The interpretation of the flow reactor experiments is complicated by loss of radicals on the quartz surface. Previous flow reactor experiments on oxidation of moist CO under conditions ranging from lean to slightly fuel-rich [e.g., 22,33,37] have shown no indications of reactions on the quartz surface, perhaps because SiO defect sites have been capped by H_2O. However, in the present work with higher reactant levels and more fuel-rich conditions we found indications of radical recombination on the reactor walls. Without loss of radicals on the surface, the modeling predictions tended to overpredict conversion of CO to CO_2 under very reducing conditions. This difference could not be explained in terms of uncertainties in the reaction mechanism, since the CO/H_2 subset is quite well established. Consequently, we attributed the discrepancy to surface reactions. To account for this in the modeling we included hydrogen atom recombination kinetics at the surface, using an apparent recombination efficiency and based on the work of Kim and Boudart [38]. They measured the recombination probability of hydrogen atoms on quartz in the 300–1250 K temperature range. We have used their recommended sticking coefficient for the 700–1250 K range of $0.48 \times \exp(-4930/T)$ to obtain the apparent recombination factor. The flow reactor experiments were then interpreted in terms of plug-flow calculations (SENKIN), using a hydrogen atom loss rate derived from two-dimensional boundary-layer calculations with surface chemistry (CRESLAF).

Table II Thermochemical Data for Selected Species (Units: kcal, mol)

Species	Hf (298)	S (298)	Cp300	Cp400	Cp500	Cp600	Cp800	Cp1000	Cp1500
NH	85.21	43.30	6.96	6.98	7.00	7.04	7.21	7.48	8.06
HNO	23.80	52.73	8.26	8.84	9.36	9.84	10.76	11.48	12.49
SO	1.20	53.02	7.22	7.55	7.84	8.08	8.43	8.62	8.95
SO_2	−70.95	59.30	9.54	10.41	11.12	11.71	12.55	13.03	13.61
SO_3	−94.60	61.35	12.17	13.76	15.05	16.07	17.45	18.16	19.02
HSO	−5.40	57.81	9.01	9.95	10.72	11.35	12.23	12.73	13.34
HOSO	−57.70	67.48	11.87	13.43	14.56	15.37	16.40	17.06	18.09
HSO_2	−33.80	63.69	11.94	13.68	14.99	15.98	17.28	18.05	18.98

RESULTS AND DISCUSSION

The results from the JSR experiments are presented in Figs. 1–4 together with the modeling results (solid lines). We studied the reduction of NO as a function of temperature over the range 800–1400 K. The initial mole fractions of CO and H_2 were identical and equal to 2000, 6500, and 6850 ppm. The concentration of NO was 0 or 950 ppm, while that of SO_2 was 0, 950, 1000, or 5000 ppm. The residence time was 120 ms. The equivalence ratio was calculated according to Eq. (1).

$$\phi = (\text{Fuel}\%/\text{O}_2\%)/(\text{Fuel}\%/\text{O}_2\%)_{\text{at } \phi=1} \qquad (1)$$

Consequently, the amount of oxygen introduced in the system via NO or SO_2 was not taken into account in the calculation of ϕ. Concentration profiles for reactants (CO, H_2, O_2, NO, and SO_2) and final products (H_2O, CO_2) were obtained.

The reduction of NO by the CO–H_2 mixture is insignificant in the investigated temperature range. However, addition of NO and SO_2 has a significant effect on the oxidation rate of the CO–H_2 mixture: under fuel-lean conditions, the presence of NO enhances oxidation below 1000 K whereas SO_2 has an inhibiting effect; under stoichiometric and fuel-rich conditions, both NO and SO_2 inhibit the oxidation of the CO–H_2 mixture.

In general, the proposed kinetic scheme is able to simulate well the measured concentration profiles shown in Figs. 1–4. For this reason, we use with some confidence rate-of-production (R with positive sign) and rate-of-consumption (R with negative sign) analysis, as well as first-order sensitivity analysis, to interpret the results. Below the interaction of NO and SO_2 with the CO–H_2 oxidation chemistry is discussed in more detail.

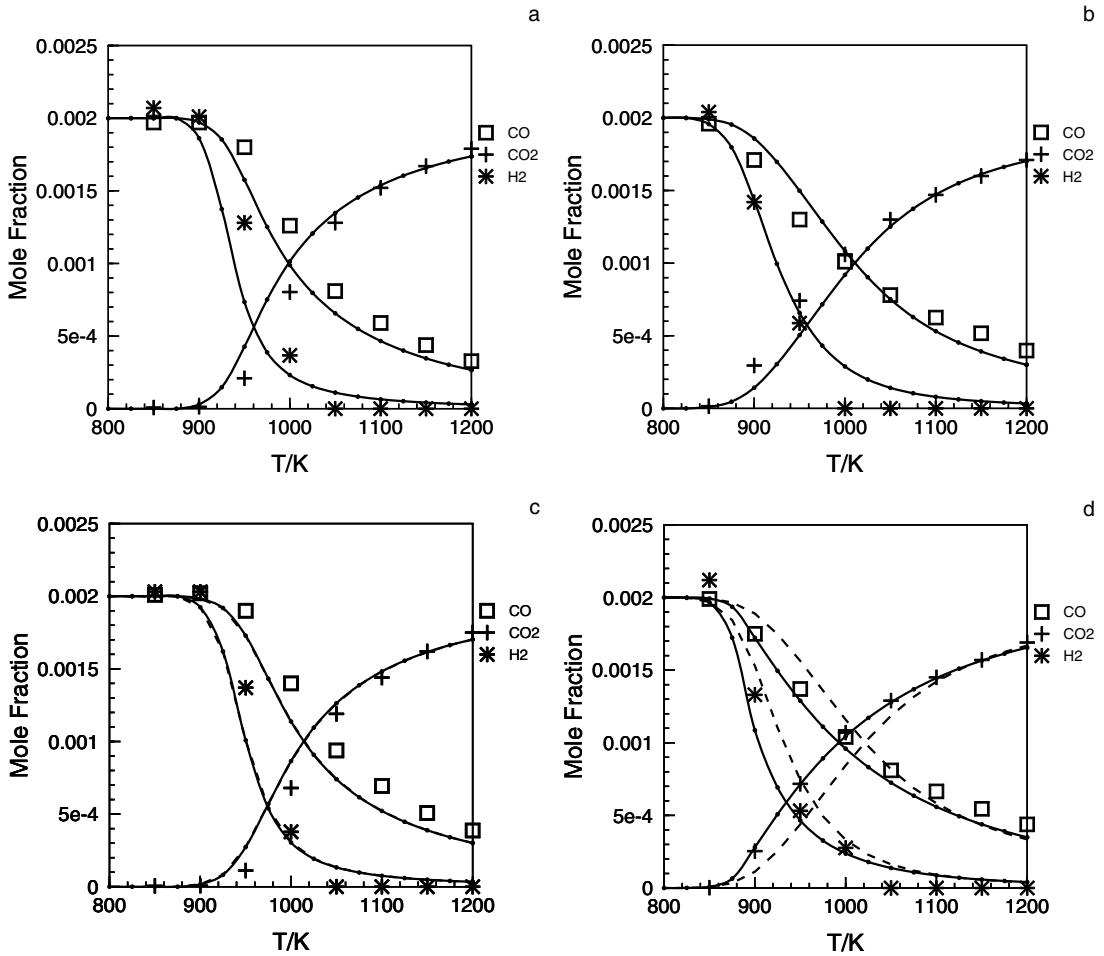

Figure 1 Fuel-lean conditions: 2000 ppm of CO and 2000 ppm of H_2, $\phi = 0.1$, residence time = 120 ms: (a) oxidation of a CO–H_2 mixture; (b) oxidation of a CO–H_2 mixture with 1000 ppm of NO; (c) oxidation of a CO–H_2 mixture with 950 ppm of SO_2; (d) oxidation of a CO–H_2 mixture with 1000 ppm of NO and 950 ppm of SO_2.

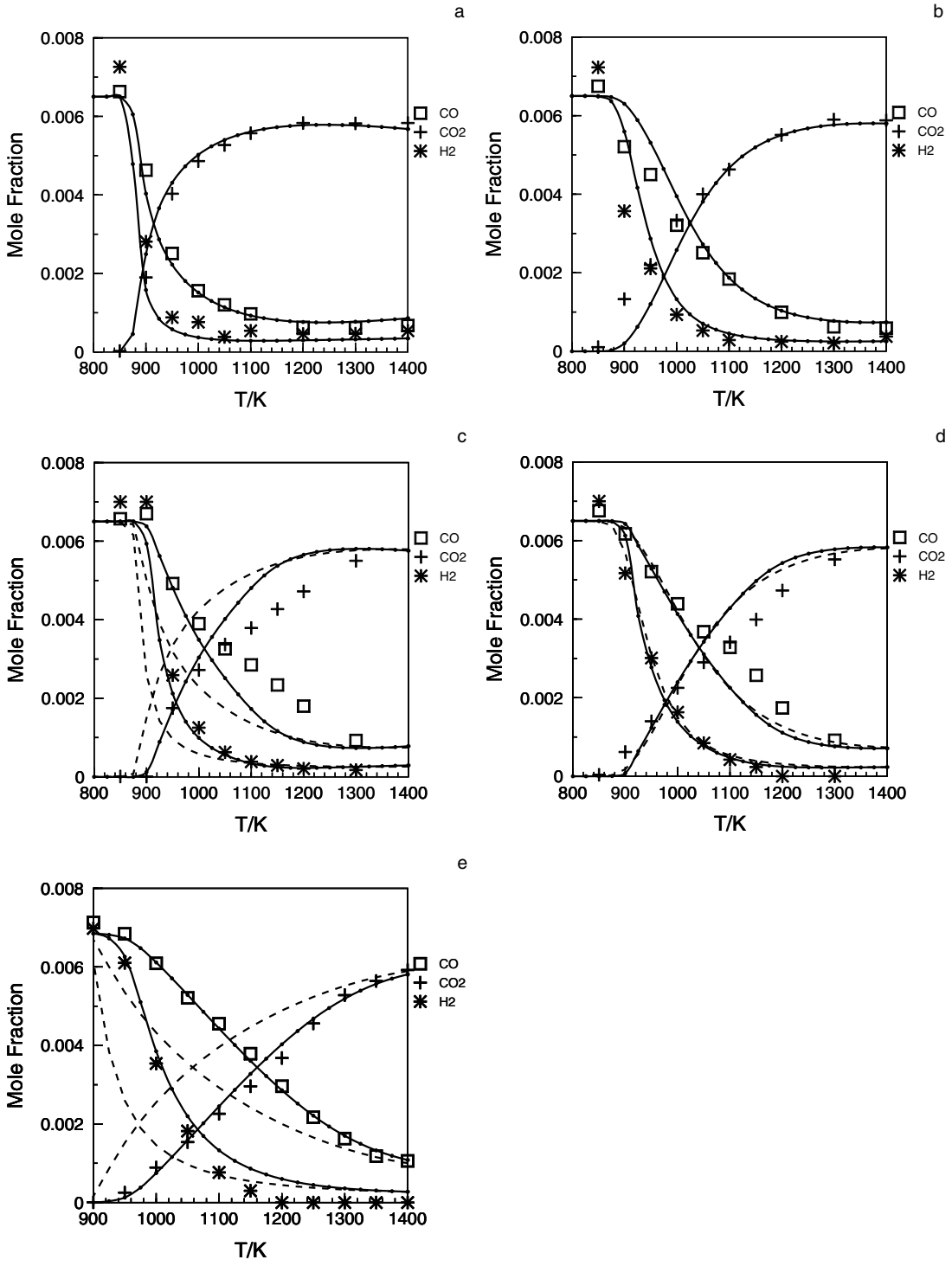

Figure 2 Stoichiometric conditions: 6500 ppm of CO and 6500 ppm of H_2, $\phi = 1$, residence time = 120 ms: (a) oxidation of a CO–H_2 mixture; (b) oxidation of a CO–H_2 mixture with 950 ppm of NO; (c) oxidation of a CO–H_2 mixture with 950 ppm of SO_2; (d) oxidation of a CO–H_2 mixture with 950 ppm of NO and 950 ppm of SO_2; (e) oxidation of a CO–H_2 mixture with 5000 ppm of SO_2.

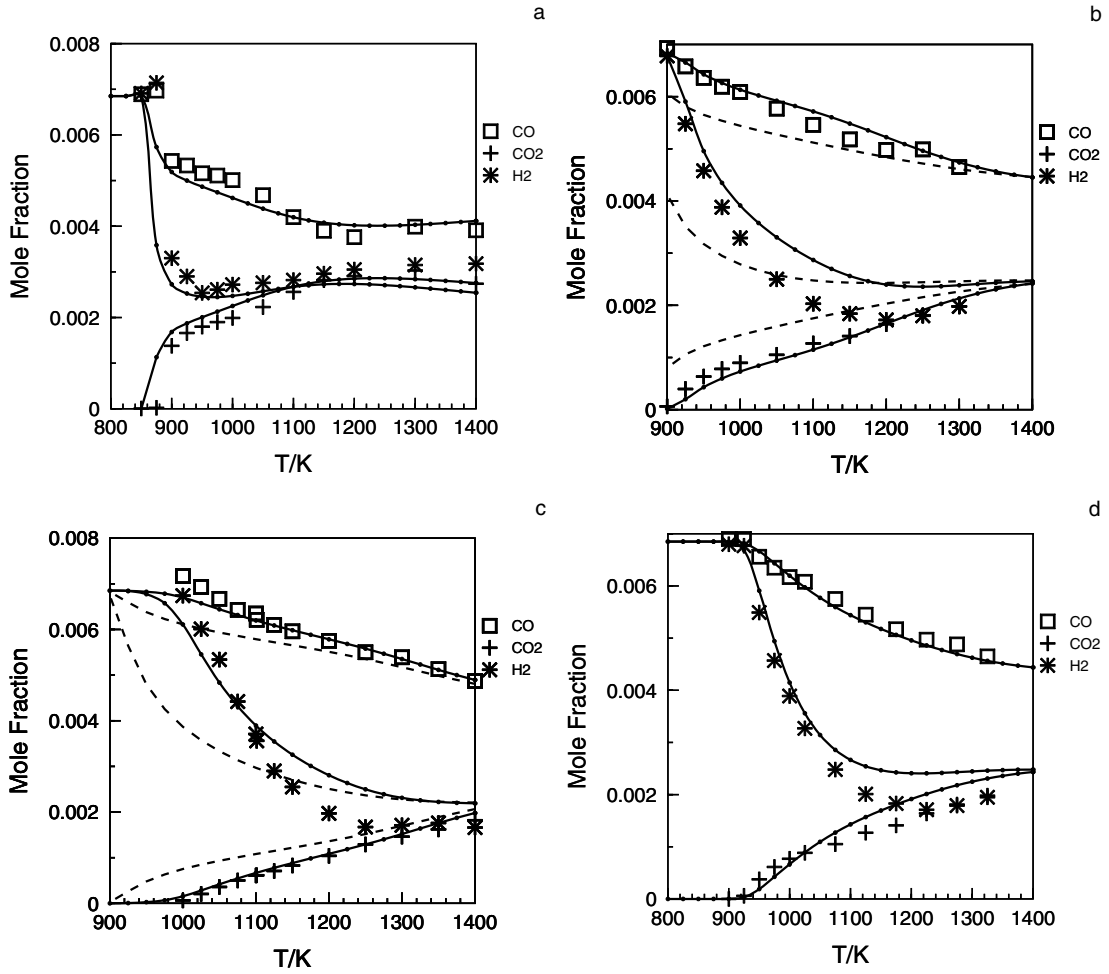

Figure 3 Fuel-rich conditions: 6850 ppm of CO and 6850 ppm of H_2, $\phi = 2.0$, residence time = 120 ms: (a) oxidation of a CO–H_2 mixture; (b) oxidation of a CO–H_2 mixture with 1000 ppm of SO_2; (c) oxidation of a CO–H_2 mixture with 5000 ppm of SO_2; (d) oxidation of a CO–H_2 mixture with 1000 ppm of NO.

Effect of NO on CO–H_2 Oxidation

Under fuel-lean conditions the addition of NO promotes the oxidation rate for the CO–H_2 mixture below 1000 K (Fig. 1b). This trend is consistent with results obtained under flow reactor conditions for CO [37], CH_2O [39], and a range of hydrocarbons [40–44]. The modeling shows that below 1000 K in fuel-lean conditions, reactions with NO contribute strongly to the production of OH. At 900 K and $\phi = 0.1$, the rate of production of OH is about four times higher when NO is added (conditions of Figs. 1a and 1b).

(141) $NO + HO_2 \Leftrightarrow NO_2 + OH$ $R(OH) = 0.401$

(146) $NO_2 + H \Leftrightarrow NO + OH$ $R(OH) = 0.396$

(267) $O + H_2 \Leftrightarrow OH + H$ $R(OH) = 0.057$

(268) $H + O_2 \Leftrightarrow OH + O$ $R(OH) = 0.134$

In particular, reaction (141) is important for the enhanced fuel oxidation rate, since this step forms OH from the comparatively unreactive HO_2 radical. At 1100 K, HO_2 is no longer formed in significant quantities and the rates of production for OH are almost identical with and without NO added.

Under stoichiometric (Fig. 2b) and fuel-rich conditions (Fig. 3b), presence of NO inhibits, rather than enhances, the oxidation of CO and H_2. This is due to the increasing importance of chain-terminating reactions. At 1200 K and stoichiometric conditions (Fig. 2b), the reaction sequence

(143) $NO + H + M \Leftrightarrow HNO + M$ $R(NO) = -0.762$

(126) $HNO + H \Leftrightarrow NO + H_2$ $R(HNO) = -0.782$

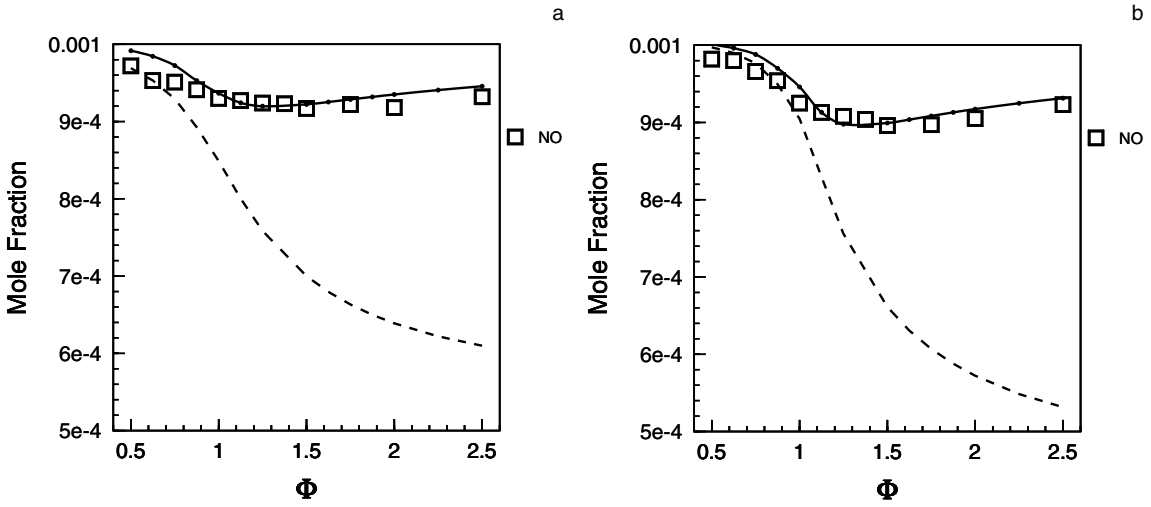

Figure 4 The reduction of NO by a CO–H_2 mixture. The effect of including NH + H_2O and NH + CO_2 reactions is shown as a dotted line whereas the modeling using the baseline mechanism is depicted as a full line (conditions: (a) 1100 K, 1000 ppm of NO, $t = 0.12$ s, 6500 ppm of hydrogen and 6500 ppm of CO oxidation; (b) 1400 K, 1000 ppm of NO, $t = 0.12$ s, 6500 ppm of hydrogen and 6500 ppm of CO oxidation.

corresponding to the overall reaction H + H = H_2, causes a strong inhibition. Under fuel-rich conditions, the inhibition of NO (Fig. 3d) by this reaction sequence is even stronger owing to the increased importance of the hydrogen atom as chain carrier.

The ability of CO and H_2 to reduce NO is quite important for the reburn potential of gases such as biomass volatiles that are characterized by a low hydrocarbon content [18]. Of particular interest in the present work has been to assess the importance of reactions that form a pathway from HNO to NH, allowing for a subsequent reduction of NO by the NH_i radical pool. The reaction

$$(-85)\quad \mathrm{HNO + H \Leftrightarrow NH + OH},$$

which competes with reaction (126) is typically the major pathway from HNO to NH under reducing conditions. However, reaction (−85) is only competitive at comparatively high temperatures and does not result in a significant reduction of NO under the present conditions. Two alternative pathways from HNO to NH are the reactions

(a) $\mathrm{HNO + CO \Leftrightarrow NH + CO_2}$
(b) $\mathrm{HNO + H_2 \Leftrightarrow NH + H_2O}$

The reverse of these reactions, attack of NH on CO_2 (-a) and H_2O (-b), have been studied at high temperatures in a shock tube by Rohrig and Wagner [17]. They found the reactions to be relatively fast. The products, HNO and CO/H_2, were not detected but proposed based on the fact that most alternative product channels were too endothermic to come into consideration. The reactions (a) and (b) are both exothermic, and with the rate constants determined by Rohrig and Wagner, they are also both comparatively fast. The reactions were not included in our mechanism since results from a flow reactor study [18] on reduction of NO by CO and H_2, respectively, showed no indication of a fast conversion of HNO to NH. However, the present measurements obtained under reducing conditions with relatively high levels of CO and H_2 are better suited than the flow reactor experiments for evaluating the potential importance of reactions (a) and (b).

Figure 4 compares the experimental data and modeling predictions for reduction of NO by the CO/H_2 mixture as function of equivalence ratio and temperature. The modeling predictions are conducted both with the original mechanism (solid lines) and with a mechanism (dashed lines) extended with reactions (a) and (b) included in the mechanism, with rate constants proposed by Rohrig and Wagner [17]. The experimental results show a modest reduction of about 5–10% of NO under reducing conditions. This level of reduction is in good agreement with modeling predictions of the original mechanism. The extended mechanism, however, grossly overpredicts the reduction of NO under stoichiometric to fuel-rich conditions and appears to be incompatible with the measurements. It was not possible by reasonable modifications to the mechanism to bring modeling predictions with the extended mechanism into agreement with our experimental results. We take this to indicate that reactions (a) and (b) do not occur to a significant extent under the investigated conditions.

The indication that a fast pathway from HNO to NH by reaction with H_2O and CO_2 does not exist has implications for our understanding of the reburning chemistry. This limits the predicted NO reduction by non-hydrocarbon fuels such as CO and H_2 under reducing conditions and not too high temperatures. Also modeling of the nitrogen chemistry occurring in nonpremixed flames is affected by the exclusion of these two reactions [19]. The reason for the discrepancy of the present results compared to the work of Rohrig and Wagner is not clear. One possible explanation is that the reactions of NH with CO_2 and H_2O detected by Rohrig and Wagner do not lead to formation of HNO as proposed, but to another set of products. However, more work is required to confirm this.

Effect of SO_2 on CO–H_2 Oxidation

Under fuel-lean conditions the addition of SO_2 results in a small inhibition of the oxidation of CO and H_2 (Fig. 1c). According to the modeling, at 1000 K, this is mostly due to the following sequence of reactions.

(7) $SO_2 + O\,(+M) \Leftrightarrow SO_3\,(+M)$
$R(SO_2) = -0.492$

(58) $H + SO_2 + M \Leftrightarrow HOSO + M$
$R(SO_2) = -0.494$

(64) $SO_3 + HO_2 \Leftrightarrow HOSO_2 + O_2$
$R(SO_3) = -0.802$

(8) $SO_2 + OH\,(+M) \Leftrightarrow HOSO_2\,(+M)$
$R(HOSO_2) = -0.998$

(57) $HOSO + O_2 \Leftrightarrow HO_2 + SO_2$
$R(HOSO) = -0.996$

The result of reactions (7), (−8), and (64) is $O + HO_2 = OH + O_2$ and of reactions (58) and (57) is $H + O_2 = HO_2$ which corresponds to a reduction of the radical pool but not a strong inhibition, in agreement with experiments. The small inhibition of the fuel oxidation caused by SO_2 under lean conditions is in agreement with results from flow reactor experiments on moist oxidation of CO with and without SO_2 [22,33].

Under stoichiometric (Fig. 2c) and fuel-rich conditions (Fig. 3c), the inhibition of the oxidation of CO and H_2 by SO_2 is more pronounced. This is due to the increasing importance of hydrogen atoms as chain carriers. At 1200 K and stoichiometric conditions (Fig. 2c), the reaction sequence

(58) $H + SO_2 + M \Leftrightarrow HOSO + M$
$R(SO_2) = -0.914$

(14) $HOSO + H \Leftrightarrow SO_2 + H_2$
$R(HOSO) = -0.702$

(57) $HOSO + O_2 \Leftrightarrow HO_2 + SO_2$
$R(HOSO) = -0.280$

is equivalent to $H + H = H_2$ [(58) + (14)] whereas (58) + (57) is equivalent to $H + O_2 = HO_2$. Under fuel-rich conditions, the inhibition by SO_2 (Fig. 3b) is even stronger because of the increased importance of reactions (58) and (14).

The strong inhibiting effect of SO_2 under stoichiometric and fuel-rich conditions was not observed in the recent flow reactor study on moist CO oxidation by Alzueta et al. [22]. They found that under stoichiometric conditions SO_2 actually promoted CO oxidation, while under reducing conditions presence of SO_2 caused only a slight inhibition of the CO oxidation rate. A number of differences in the experimental conditions may conceivably contribute to the different trends observed in the present experiments compared to those of Alzueta et al. These differences include fuel (CO/H_2 in this study versus moist CO), reactant concentrations (higher levels in the present study), and reactor type (JSR vs. LFR). However, to further investigate this issue, additional flow reactor experiments were conducted as part of the present study. In these experiments, reactant compositions similar to those employed in the JSR experiments were used.

The results of the flow reactor experiments are shown in Fig. 5. Figure 5a compares experimental results and modeling predictions for the effect of SO_2 on CO/H_2 oxidation under stoichiometric conditions, while Fig. 5b shows similar results for fuel-rich conditions. Only under the conditions of Fig. 5b in the absence of SO_2 are surface reactions predicted to be significant; in the other conditions studied radical loss on the reactor surface is small or negligible.

The presence of SO_2 under both stoichiometric and reducing conditions causes a considerable inhibition of the fuel oxidation. This behavior is very similar to that observed in the jet-stirred experiments (Figs. 2c and 3c), but quite different from the results obtained in the previous flow reactor study [22]. Apparently the differences between this and the earlier study [22] are caused primarily by differences in reactant composition, rather than reactor technique.

The consistency between the JSR results and the flow reactor results of the present work is confirmed by the good agreement of both sets of experimental data with the modeling predictions. The inhibiting effect of SO_2 found in the present experimental work is explained in terms of the recombination of hydrogen atoms with SO_2 (58) followed by reaction of HOSO

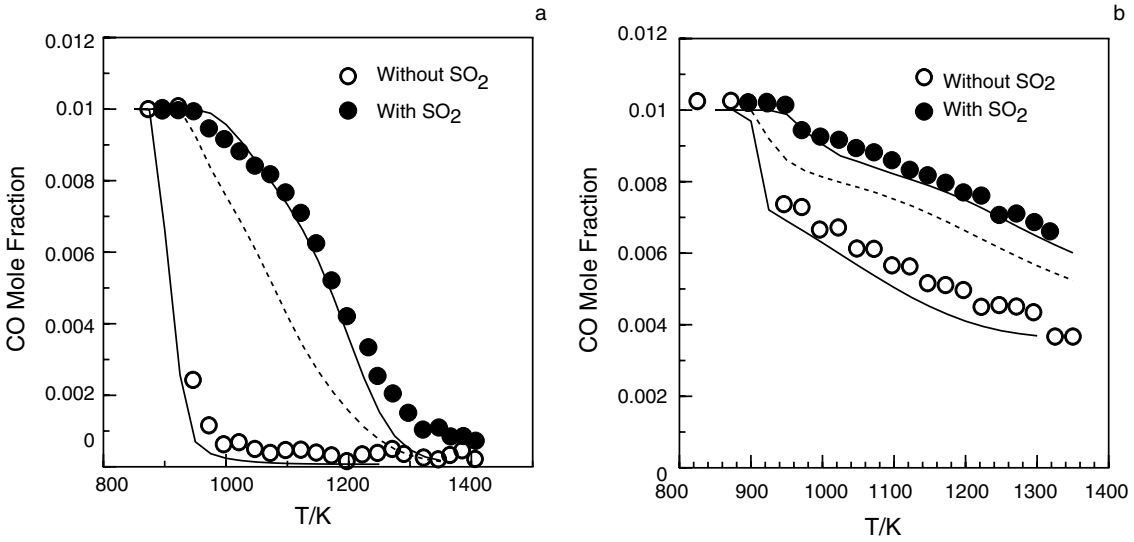

Figure 5 The effect of SO_2 on the oxidation of a CO–H_2 mixture in a plug-flow reactor. Initial conditions: (a) CO = 1.0%, H_2 = 1.0%, O_2 = 1.0%, H_2O = 2.0%, balance N_2, without and with SO_2 = 1.2%, residence time is 192.7/*T* or 192.3/*T*; (b) CO = 1.0%, H_2 = 1.0%, O_2 = 0.5%, H_2O = 2.0%, balance N_2, without and with SO_2 = 0.3%, residence time is 192.7/*T* or 192.3/*T*.

with H, recycling the sulfur to SO_2. This reaction sequence is apparently the only mechanism that can explain the experimental observations. However, to bring the modeling predictions in accordance with the measurements, a very high rate for H + SO_2 + M (58) is required. With the present mechanism, the reactor data supports a rate constant that is 5–10 times higher than the theoretical estimate of Goumri et al. [20] and 50–100 times higher than the upper limit derived from the previous flow reactor investigation [22].

The value used for k_{58} in the present work is the low pressure limit proposed by Goumri et al. However, according to the estimate of Goumri et al., reaction (58) should be in the fall-off region under the current conditions and significantly slower than the low pressure limit (see [20]). Modeling predictions taking the fall-off behavior of (58) into account, using the high and low pressure limits from Goumri et al. [20] together with the Troe coefficient from [22] are shown in Figs. 2c, 3c, and 5 as dashed lines. Using these coefficients for k_{58} the model clearly underpredicts the effect of SO_2. The discrepancy is even more pronounced if the value of k_{58} from Alzueta et al. [22] is used (not shown).

We have currently no explanation for the discrepancy with theory and with previous experimental work. Some of the difference may be attributed to the uncertainty in rate constants and products for reactions of SO, HSO and HOSO. However, it can be concluded that the JSR experiments and the present flow reactor experiments, which are internally consistent, both support a high rate for the H + SO_2 recombination reaction.

Combined Effect of NO and SO_2 on CO–H_2 Oxidation

The JSR experiments show that addition of SO_2 inhibits oxidation of a CO–H_2 mixture over the full range of stoichiometries investigated, i.e., at $\phi = 0.1$, 1, and 2. The effect of NO is more complex. Inhibition is the dominating effect at stoichiometric and rich conditions ($\phi =$ 1 and 2), whereas at lean conditions ($\phi = 0.1$) promotion is observed below 1000 K and inhibition above this temperature. Addition of both NO and SO_2 primarily augments the inhibiting effect of SO_2. Both components act to suppress the concentrations of primarily H and O atoms in the radical pool. Under stoichiometric and fuel-rich conditions these effects are largely additive. Under lean conditions the interaction is more complex because of the ability of NO to convert HO_2 to OH.

CONCLUSION

New experimental results have been obtained for the interaction of NO and SO_2 with oxidation of a CO–H_2 mixture. The experiments were performed using a JSR and a LFR at atmospheric pressure and temperatures from 800 to 1400 K, under conditions ranging from fuel-lean to fuel-rich. The experimental data were interpreted in terms of a detailed chemical kinetic model.

Under fuel-lean conditions, the addition of NO promotes the oxidation of the CO–H_2 mixture below 1000 K, whereas the addition of SO_2 has a small

inhibiting effect. Under stoichiometric and fuel-rich conditions, both NO and SO_2 inhibit the oxidation of the CO–H_2 mixture. An overall reasonable agreement between the experimental results and the modeling was obtained. According to the present kinetic modeling, the main path to inhibition by NO is $NO + H + M = HNO + M$ followed by $HNO + H = NO + H_2$, whereas that involving SO_2 is $H + SO_2 + M = HOSO + M$ followed by $HOSO + H = H_2 + SO_2$. The model and the data indicate that the inhibiting effects of NO and SO_2 increase as the equivalence ratio increases. The results show that a CO–H_2 mixture has a limited NO reduction potential in the investigated temperature range and rule out a significant conversion of HNO to NH through reactions like $HNO + CO \Leftrightarrow NH + CO_2$ or $HNO + H_2 \Leftrightarrow NH + H_2O$. The considerable chain-terminating effect of SO_2 observed under stoichiometric and reducing conditions in both type of reactors support a high rate constant for the $H + SO_2 + M \Leftrightarrow HOSO + M$ reaction.

The authors thank Art Fontijn and Bill Anderson for helpful discussions on the reactions of NH with CO_2 and H_2O.

BIBLIOGRAPHY

1. Wendt, J. O. L.; Sterling, C. V.; Matovich, M. A. Proc Combust Inst 1973, 14, 897.
2. Smoot, L. D.; Hill, S. C.; Xu, H. Prog Energy Combust Sci 1998, 24, 385.
3. Alzueta, M. U.; Glarborg, P.; Dam-Johansen, K. Combust Flame 1997, 25, 109.
4. Dagaut, P.; Lecomte, F.; Chevailler, S.; Cathonnet, M. Combust Sci Technol 1998, 139, 329.
5. Glarborg, P.; Alzueta, M. U.; Dam-Johansen, K.; Miller, J. A. Combust Flame 1998, 115, 1.
6. Prada, L.; Miller, J. A. Combust Sci Technol 1998, 132, 225.
7. Harding, N. S.; Adams, B. R. Biomass Bioenergy 2000, 19, 429.
8. Sander, B. Biomass Bioenergy 1997, 12, 177.
9. Jenkins, B. M.; Baxter, L. L.; Miles, T. R. Jr. Fuel Process Technol 1998, 54, 17.
10. Werther, J.; Saenger, M.; Hartge, E. U. Prog Energy Combust Sci 2000, 26, 1.
11. Chagger, H. K.; Goddard, P. R.; Murdoch, P.; Williams, A. Fuel 1991, 70, 1137.
12. Dagaut, P.; Cathonnet, M. In Proceedings of the 6th European Conference on Industrial Furnaces and Boilers, Lisbon, Portugal, 2–5 April 2002.
13. Dagaut, P.; Lecomte, F. Fuel 2003, 82, 1033.
14. Storm, C.; Spliethoff, H.; Hein, K. R. G. In Proceedings of the 5th European Conference on Industrial Furnaces and Boilers, Porto, Portugal, 2–5 April 2000; pp. 689–700.
15. Zanzi, R.; Sjöström, K.; Björnbom, E. Fuel 1996, 75, 545.
16. Zanzi, R.; Sjöström, K.; Björnbom, E. Biomass Bioenergy 2002, 23, 357.
17. Rohrig, M.; Wagner, H. G. Proc Combust Inst 1994, 25, 975.
18. Glarborg, P.; Kristensen, P. G.; Johansen, K.; Alzueta, M. U.; Millera, A.; Bilbao, R. Energy Fuels 2000, 14, 828.
19. Sullivan, N.; Jensen, A.; Glarborg, P.; Day, M. S.; Grcar, J. F.; Bell, J. B.; Pope, C. J.; Kee, R. J. Combust Flame 2002, 131, 285.
20. Goumri, A.; Rocha, J.-D. R.; Laakso, D.; Smith, C. E.; Marshall, P. J Phys Chem A 1999, 103, 11328.
21. Baulch, D. L.; Drysdale, D. D.; Duxbury, J.; Grant, S. J. Evaluated Data for High Temperature Reactions; Butterworth: London, 1976; Vol. 3.
22. Alzueta, M. U.; Bilbao, R.; Glarborg, P. Combust Flame 2001, 127, 2234.
23. Dagaut, P.; Cathonnet, M.; Rouan, J.-P.; Foulatier, R.; Quilgars, A.; Boettner, J.-C.; Gaillard, F.; James, A. J Phys E: Sci Instrum 1985, 19, 207.
24. Kristensen, P. G.; Glarborg, P.; Dam-Johansen, K. Combust Flame 1996, 10, 211.
25. Glarborg, P.; Kee, R. J.; Grcar, J. F.; Miller, J. A. Sandia Report SAND86-8209, Sandia National Laboratories, 1986.
26. Lutz, A. E.; Kee, R. J.; Miller, J. A. Sandia Report SAND87-8248, Sandia National Laboratories, 1990.
27. Coltrin, M. E.; Kee, R. J. Sandia Report SAND93-0478, Sandia National Laboratories, 1993.
28. Kee, R. J.; Rupley, F. M.; Miller, J. A. Sandia Report SAND89-8009, Sandia National Laboratories, 1989.
29. Coltrin, M. E.; Kee, R. J.; Rupley, F. M. Sandia Report SAND90-8003, Sandia National Laboratories, 1990.
30. Tan, Y.; Dagaut, P.; Cathonnet, M.; Boettner, J.-C.; Bachman, J.-S.; Carlier, P. Proc Combust Inst 1994, 25, 1563.
31. Tan, Y.; Dagaut, P.; Cathonnet, M.; Boettner, J.-C. J Chim Phys 1995, 92, 726.
32. Hori, M.; Matsunaga, N.; Marinov, N.; Pitz, W.; Westbrook, C. Proc Combust Inst 1998, 27, 389. (See also www-cms.llnl.gov/combustion/combustion_home.html.)
33. Glarborg, P.; Kubel, D.; Dam-Johansen, K.; Chiang, H.-M.; Bozzelli, J. W. Int J Chem Kinet 1996, 28, 773.
34. Tan, Y.; Dagaut, P.; Cathonnet, M.; Boettner, J.-C. Combust Sci Technol 1994, 102, 21.
35. Kee, R. J.; Rupley, F. M.; Miller, J. A. Sandia Report SAND87-8215, Sandia National Laboratories, 1991.
36. Dagaut, P.; Lecomte, F.; Chevailler, S.; Cathonnet, M. Combust Sci Technol 1999, 148, 27.
37. Glarborg, P.; Kubel, D.; Kristensen, P. G.; Hansen, J.; Dam-Johansen, K.; Combust Sci Technol 1995, 110/111, 461.

38. Kim, Y. C.; Boudart, M. Langmuir 1991, 7, 2999.
39. Glarborg, P.; Alzueta, M. U.; Kjaergaard, K.; Dam-Johansen, K. Combust Flame 2003, 132, 629.
40. Bromly, J. H.; Barnes, F. J.; Muris, S.; You, X.; Haynes, B. S. Combust Sci Technol 1996, 115, 259.
41. Bendtsen, A. B.; Glarborg, P.; Dam-Johansen, K. Combust Sci Technol 2000, 151, 31.
42. Bromly, J. H.; Barnes, F. J.; Mandyczewsky, R.; Edwards, T.; Haynes, B. S. Proc Combust Inst 1992, 24, 899.
43. Doughty, A.; Barnes, F. J.; Bromly, J. H.; Haynes, B. S. Proc Combust Inst 1996, 26, 599.
44. Hjuler, K.; Glarborg, P.; Dam-Johansen, K. Ind Eng Chem Res 1995, 34, 1882.